Volume 5 | Number 40 | 28 October 2017 | Pages 21031–21580

Journal of Materials Chemistry A

Materials for energy and sustainability

rsc.li/materials-a

ISSN 2050-7488

ROYAL SOCIETY OF CHEMISTRY

PAPER

Qingwen Li, Yagang Yao *et al.*

Constructing hierarchical dandelion-like molybdenum–nickel–cobalt ternary oxide nanowire arrays on carbon nanotube fiber for high-performance wearable fiber-shaped asymmetric supercapacitors

Journal of Materials Chemistry A

PAPER

View Article Online
View Journal | View Issue

Cite this: J. Mater. Chem. A, 2017, 5, 21153

Constructing hierarchical dandelion-like molybdenum–nickel–cobalt ternary oxide nanowire arrays on carbon nanotube fiber for high-performance wearable fiber-shaped asymmetric supercapacitors†

Juan Sun,[abc] Qichong Zhang,[a] Xiaona Wang,[a] Jingxin Zhao,[a] Jiabin Guo,[a] Zhenyu Zhou,[a] Jun Zhang,[a] Ping Man,[a] Jing Sun,[c] Qingwen Li*[ab] and Yagang Yao*[a]

Emerging fiber-shaped supercapacitors have been considered as promising new-state energy storage devices for next-generation wearable electronics. However, the limited energy densities arising from the small specific capacitance and low operating voltage severely restrict their practical application. Here, we develop a facile and effective method to directly grow dandelion-like molybdenum–nickel–cobalt ternary oxide (MNCO) nanowire arrays (NWAs) on carbon nanotube fiber (CNTF) with a high specific capacitance of 490.7 F cm^{-3} (1840 mF cm^{-2}) at a current density of 1 mA cm^{-2}. Benefiting from the three-dimensional nanostructure, high conductivity and excellent pseudocapacitance properties, we successfully fabricate a fiber-shaped asymmetric supercapacitor (FASC) with a maximum operating voltage of 1.6 V, which is assembled by twisting a MNCO/CNTF positive electrode and thin carbon-coated VN NWAs on CNTF negative electrode together with KOH/poly(vinyl alcohol) (PVA) as the gel electrolyte. The optimized FASC delivers a remarkable specific capacitance of 62.3 F cm^{-3} (233.7 mF cm^{-2}) and an exceeding energy density of 22.2 mW h cm^{-3} (83.1 μW h cm^{-2}). Additionally, it exhibits outstanding flexibility with capacitance retention maintained at 90.2% after bending 3500 times. Thus, the high performance MNCO/CNTF electrode opens a new avenue to fabricate high-performance FASCs for next-generation wearable energy storage devices.

Received 20th July 2017
Accepted 14th August 2017

DOI: 10.1039/c7ta06353a

rsc.li/materials-a

Introduction

As a new type of energy storage device for portable and wearable electronics, flexible supercapacitors have been attracting tremendous attention owing to their high power density, fast charge/discharge capability, long cycle life and outstanding flexibility.[1–9] Compared with conventional two-dimensional supercapacitors,[1,2,10] fiber-shaped supercapacitors (FSCs) with tiny volume, extraordinary flexibility and remarkable weavability are particularly intriguing.[11–16] Recently, various fibrous materials have been widely applied as conductive substrates to fabricate high-performance FSCs.[16–19] Among these FSCs, carbon nanotube fibers (CNTFs) are identified as promising candidates for fibrous electrodes due to their extraordinary structural flexibility, remarkable mechanical strength and high electrical conductivity.[20–22]

Although extensive efforts have been made to develop high-performance FSCs, it is still a key challenge to obtain high energy density without sacrificing their power density and cycle life for their practical application.[11–20] According to $E = 1/2CV^2$, we can clearly see that the energy density (E) can be improved by increasing the specific capacitance (C) or extending the operating voltage (V).[15,17,23] Thus, an effective strategy to increase the energy density is to fabricate asymmetric supercapacitors which make full utilization of the operational windows of both positive and negative electrode materials.[24–32] However, it is difficult for asymmetric FSCs with low energy density that results from the material's low specific capacitance to meet the ever-growing energy demand in wearable electronics. Therefore, it is highly desirable to synthesize highly capacitive electrode materials.

[a]Division of Advanced Nanomaterials, Key Laboratory of Nanodevices and Applications, CAS Center for Excellence in Nanoscience, Suzhou Institute of Nano-tech and Nano-bionics, Chinese Academy of Sciences, Suzhou 215123, P. R. China. E-mail: ygyao2013@sinano.ac.cn; qwli2007@sinano.ac.cn

[b]School of Physical Science and Technology, ShanghaiTech University, Shanghai 200120, P. R. China

[c]The State Key Lab of High Performance Ceramics and Superfine Microstructure, Shanghai Institute of Ceramics, University of Chinese Academy of Sciences, 1295 Dingxi Road, Shanghai 200050, P. R. China

† Electronic supplementary information (ESI) available. See DOI: 10.1039/c7ta06353a

Owing to its high specific capacitance, simple and green synthesis methods and low cost, Co_3O_4 has been intensively investigated as one of the most promising positive electrode materials for high-performance supercapacitors.[33,34] However, the low conductivity that results in slow electron transfer limits the electrochemical performance of the as-fabricated supercapacitors.[35] To date, an effective strategy to improve the electrochemical performance of Co_3O_4 is to construct complex oxides ascribing to enhanced electronic conductivity and electrochemical activity with the presence of mixed valence metal cation.[36–42] Recently, Zhang and co-workers reported zinc–nickel–cobalt ternary oxide nanowire arrays that directly grew on nickel foam with a high specific capacitance of 2481.8 F g^{-1} at 1 A g^{-1}. Compared with according mono-metal oxide and binary-metal oxide, zinc–nickel–cobalt ternary oxide nanowire arrays possess higher specific capacitance due to high electrical conductivity, which is in favor of fast charge transportation at the electrode/electrolyte interface.[43] As is well known, three-dimensional hierarchical architectures can provide ultrahigh surface areas, which would benefit electrolyte access to the electrode and accelerate electron and ion transport.[8,43,44] Here, a facile and effective method was successfully developed to directly grow hierarchical dandelion-like molybdenum–nickel–cobalt ternary oxide (MNCO) nanowire arrays (NWAs) on CNTF as a novel binder-free electrode. As for the MNCO/CNTF electrode, Co and Ni exhibit ultrahigh capacitive performance and Mo can improve the electrical conductivity. Therefore, the as-prepared dandelion-like MNCO is expected to be a promising alternative to state-of-the-art positive electrode materials.

Herein, we successfully prepared a high-performance and wearable fiber-shaped asymmetric supercapacitor (FASC) with a maximum operating voltage of 1.6 V by utilizing hierarchical dandelion-like MNCO/CNTF as the positive electrode and VN@C/CNTF as the negative electrode (denoted as VN@C/CNTF//MNCO/CNTF). The optimized device exhibits a remarkable specific capacitance of 62.3 F cm^{-3} (233.7 mF cm^{-2}), a high energy density of 22.2 mW h cm^{-3} (83.1 μW h cm^{-2}) and an extraordinary power density of 2133.3 mW cm^{-3} (8000 μW cm^{-2}), which are higher than most reported values for similar FASCs. Additionally, the as-assembled devices show negligible degradation of their electrochemical performance after bending 3500 times, demonstrating their excellent flexibility. Thus, this work opens an avenue to develop high-performance fiber-shaped energy storage devices for portable and wearable electronics in the future.

Experimental section

Synthesis of hierarchical dandelion-like MNCO NWAs on CNTF

The hierarchical dandelion-like MNCO NWAs supported on CNTFs were synthesized *via* a simple two-step method including a facile hydrothermal process and a post annealing treatment. First, CNTFs were treated in O_2 plasma for 5 min at 150 W. In a typical process, 0.5296 g ammonium molybdate tetrahydrate ($(NH_4)_6Mo_7O_{24}\cdot 4H_2O$), 1.7462 g cobalt nitrate hexahydrate ($Co(NO_3)_2\cdot 6H_2O$), 0.87237 g nickel nitrate hexahydrate ($Ni(NO_3)_2\cdot 6H_2O$), 0.7207 g urea ($CO(NH_2)_2$) and 0.1482 g ammonium fluoride (NH_4F) were dissolved in 80 ml deionized water under magnetic stirring for 30 min to form a homogeneous red solution. Then the prepared aqueous solution and the pre-treated CNTFs were transferred into a 100 ml Teflon-lined stainless steel autoclave. The autoclave was sealed and kept at 130 °C for 5 h and naturally cooled down to room temperature. Thereafter, the resulting CNTFs covered with the MNCO precursor were taken out and carefully rinsed with deionized water several times and then vacuum dried at 60 °C for 12 hours. Finally, the hybrid fibers were directly annealed in a furnace at 350 °C in air for 4 hours to obtain the target samples. Simultaneously, CNTF supported Co_3O_4 NWAs were prepared *via* a similar approach for comparison.

Fabrication of FASCs

The FASC devices were assembled by utilizing hierarchical dandelion-like MNCO/CNTFs as positive electrodes and VN@C/CNTFs as negative electrodes with KOH/poly(vinyl alcohol) (PVA) gel electrolyte. The KOH/PVA gel electrolyte was prepared by mixing 11.2 g KOH and 10 g PVA in 100 ml distilled water with vigorous stirring at 95 °C for 2 h until the mixture became clear. After that, both MNCO/CNTF and VN@C/CNTF electrodes were immersed into the KOH/PVA gel electrolyte for 10 min and subsequently dried at 60 °C for 2 h. Finally, the all-solid-state device was assembled successfully by twisting these two electrodes together and allowed to dry overnight until the KOH/PVA gel electrolyte solidified completely.

Materials characterization

Morphology information of the samples was characterized utilizing a scanning electron microscope (Hitachi S-4800, 5 kV) and the microstructure was observed on a Tecnai G2 F20 S-Twin transmission electron microscope (TEM). High-resolution TEM images were recorded on an FEI Tecnai G2 20 high-resolution transmission electron microscope at an acceleration voltage of 200 kV. The crystal structure of the samples was identified utilizing a Rigaku D/MAX2500 V X-ray diffractometer (XRD) with Cu Kα radiation ($\lambda = 1.5418$ Å). The chemical composition and oxidation states were analyzed by X-ray photoelectron spectroscopy on an ESCALAB MKII X-ray photoelectron spectrometer with non-monochromatized Mg Kα X-rays as the excitation source.

Results and discussion

Fabrication, structure and morphology of MNCO

Hierarchical dandelion-like MNCO NWAs were directly grown on CNTF (Fig. S1†) *via* a simple two-step method including a facile hydrothermal approach and a subsequent annealing process. As shown in Fig. 1a, the nanowire-assembled dandelions are densely and uniformly distributed on the entire surface of CNTF. Furthermore, the magnified scanning electron microscope (SEM) image displayed in Fig. 1b clearly demonstrates that these nanowire-assembled dandelions are well arranged with a diameter of about 11.3 μm. Significantly, such

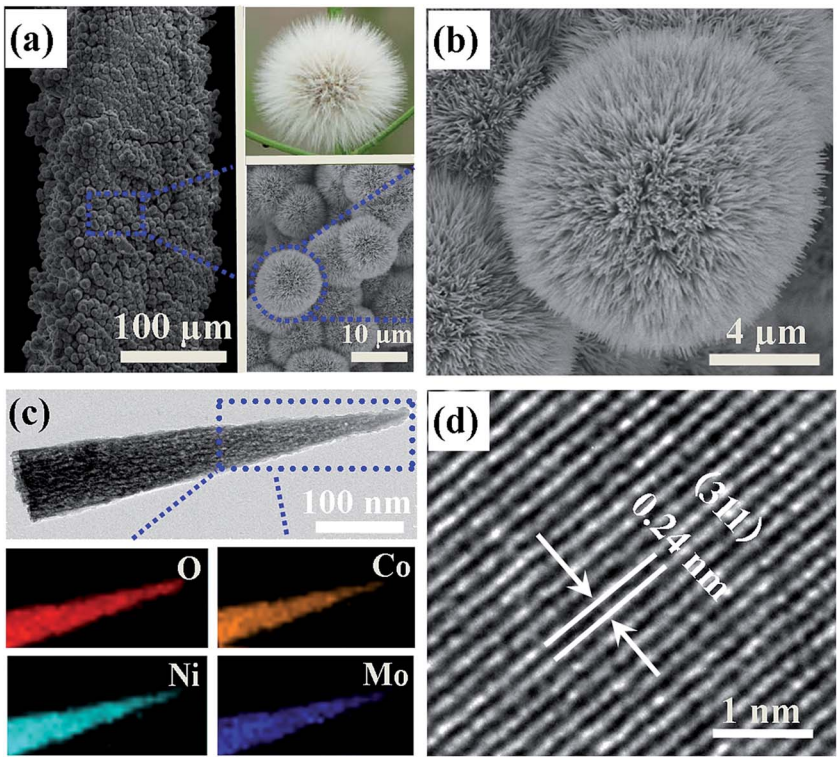

Fig. 1 (a and b) Typical SEM images of dandelion-like MNCO NWAs on CNTF at increasing magnifications. (c) TEM image and corresponding EDX mappings of Co, Ni, Mo and O for an individual MNCO nanowire. (d) High-resolution TEM image of an individual MNCO NW from (c).

a radial arrangement is able to provide an ultrahigh surface area for rapid reversible faradaic redox reactions, thus improving the electrochemical performance. Additionally, the energy-dispersive X-ray spectrometry (EDX) mapping results evidently identify that the elements Mo, Co, Ni and O are homogeneously distributed on the whole nanowire (Fig. 1c). As displayed in Fig. S2,† all X-ray diffraction (XRD) peaks of the MCNO could be indexed to the spinel Co_3O_4 phase (JCPDS 74-1656). Owing to the introduction of Mo and Ni, the diffraction peaks shift slightly and no additional peaks for other phases are observed.[43,45,46] As shown in Fig. 1d, the high-resolution transmission electron microscopy (TEM) image reveals clear lattice fringes and an interplanar spacing of about 0.24 nm, corresponding to the (311) plane of MCNO, which agrees well with the XRD result. The detailed elemental compositions and electronic states of the as-prepared MNCO are further analyzed by X-ray photoelectron spectroscopy (XPS). The survey spectrum (Fig. S3†) and high resolution XPS spectra (Fig. S4†) confirm the coexistence of Co, Ni, Mo and O, further supporting the successful preparation of MCNO electrode materials.

Electrochemical behaviors of the MNCO/CNTF electrode

The electrochemical performance of the as-fabricated electrodes was measured with a three-electrode system in 3 M KOH aqueous electrolyte. The MNCO/CNTF was directly utilized as the working electrode; a Pt wire and Ag/AgCl were selected as the counter and reference electrodes, respectively. Fig. 2a compares the galvanostatic charge–discharge (GCD) curves of pristine CNTF, Co_3O_4/CNTF and MNCO/CNTF electrodes at the same current density of 1 mA cm^{-2} at a potential sweep window of 0–0.4 V. It can be clearly seen that the pristine CNTF shows a much shorter discharge time compared with those covered with electrochemically active materials, thus indicating the negligible contribution of CNTF to the capacitance of hybrid fibers. It should be noted that the discharge time of the MNCO/CNTF electrode is evidently longer than that of the Co_3O_4/CNTF electrode (the structure and morphology of Co_3O_4 are further confirmed in Fig. S5†), indicating its enhanced specific capacitance, ascribed to the three-dimensional hierarchical nanostructure and the low equivalent series resistance in the electrochemical impedance spectroscopy (EIS) (Fig. S6†) after the introduction of Ni and Mo elements. Fig. 2b presents the cyclic voltammetry (CV) curves of the MNCO/CNTF electrode at various scan rates ranging from 1 to 10 mV s^{-1}. All curves display distinct redox peaks, indicating rapid reversible faradaic redox reactions on the surface of the electrode. The nonlinear and asymmetric GCD curves of the MNCO/CNTF electrode are obtained at different current densities from 1 to 10 mA cm^{-2}, further implying ideal pseudocapacitive properties (Fig. 2c). Fig. 2d shows the calculated areal and volumetric specific capacitances of the MNCO/CNTF electrode according to the GCD curves. Notably, a high specific capacitance of 490.7 F cm^{-3} (1840 mF cm^{-2}) can be achieved at a current density of 1 mA cm^{-2} and it still maintains 354.7 F cm^{-3} (1330 mF cm^{-2}) even at a high charge/discharge current density of 10 mA cm^{-2}, suggesting excellent rate capability. The long-term cycling

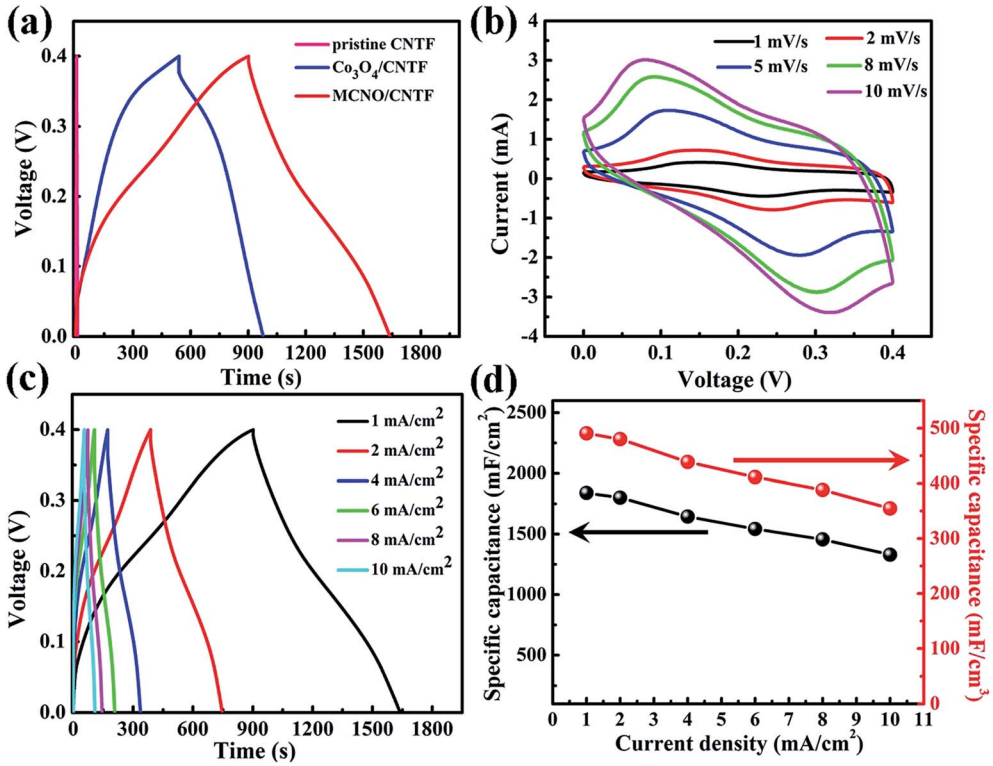

Fig. 2 (a) Comparison of the GCD curves of pristine CNTF, Co_3O_4/CNTF and MNCO/CNTF obtained at a current density of 1 mA cm^{-2}. (b) CV curves of the MNCO/CNTF electrode at various scan rates. (c) GCD curves of the MNCO/CNTF electrode at different current densities. (d) Areal and volumetric specific capacitances of the MNCO/CNTF electrode at different current densities.

performance of the MNCO/CNTF fiber electrodes was investigated by GCD analysis at a current density of 2 mA cm^{-2} (Fig. S7†). Taking the above electrochemical measurement results into consideration, it is worth noting that the MNCO/CNTF hybrid fiber can serve as an intriguing electrode for wearable supercapacitors.

Electrochemical performance of the as-assembled FASCs

To further evaluate the feasibility of the as-fabricated MNCO/CNTF electrode for practical application, a high-performance negative material is highly desirable to construct a high-energy-density asymmetric supercapacitor. Compared with various pseudocapacitive negative materials such as MoS_2,[47] MoO_2 (ref. 48) and Fe_2N,[31] vanadium nitride (VN) is considered as one of the most attractive candidates owing to its high specific capacitance (1340 F g^{-1}) and extraordinary electrical conductivity (10^6 Ω m).[20,49] In this regard, we developed a facile and effective method to directly grow well-aligned three-dimensional VN NWAs on CNTF. Subsequently, the VN NWAs were coated with a thin carbon shell (VN@C) to improve their cycling stability. The homogeneously distributed VN NWAs are demonstrated by the SEM image in Fig. S8a† and the core–shell structure of the VN@C is exhibited by the TEM images in Fig. S9.† Besides, the typical high-resolution TEM image reveals the well fitted (111) and (200) planes of VN, which agree well with the crystallites recorded by XRD (Fig. S8b†). Furthermore, the XPS results further confirm the chemical compositions and metal oxidation states (Fig. S8†). The electrochemical properties of the as-fabricated VN@C/CNTF electrode are presented in Fig. S10.† It exhibits an operating window between −1.2 and −0.2 V and a specific capacitance of 965 mF cm^{-2} at a current density of 1 mA cm^{-2}.

Based on the above results, an all-solid-state FASC was successfully prepared and the fabrication process is schematically illustrated Fig. 3. The CNTF served as a current collector and flexible electrode. First of all, the hierarchical dandelion-like MNCO/CNTF electrode was fabricated *via* a simple hydrothermal process and post annealing in air at 350 °C for 4 h. Meanwhile, VO_x NWAs were directly synthesized on CNTF by a hydrothermal approach and soaked with glucose solution for 24 h to form a thin glucose layer. Thereafter, the resulting VO_x NWAs with the thin glucose layer were annealed in ammonia at 600 °C for 2 h to prepare carbon-coated VN NWAs. Finally, the FASC was successfully assembled by twisting the MNCO/CNTF and VN@C/CNTF hybrid fibers together after coating them with a thin layer of KOH/PVA gel electrolyte, which is displayed in Fig. S11† by the corresponding digital image and low-magnification SEM image.

Fig. 4a shows the CV curves of the VN@C/CNTF and MNCO/CNTF electrodes in 3 M KOH at a scan rate of 5 mV s^{-1} to estimate the device's total voltage. Notably, the potential windows of VN@C/CNTF and MNCO/CNTF fiber electrodes are −1.2 to −0.2 V and 0 to 0.4 V, respectively. Thus, it is anticipated that the operating voltage of the as-assembled device could be extended

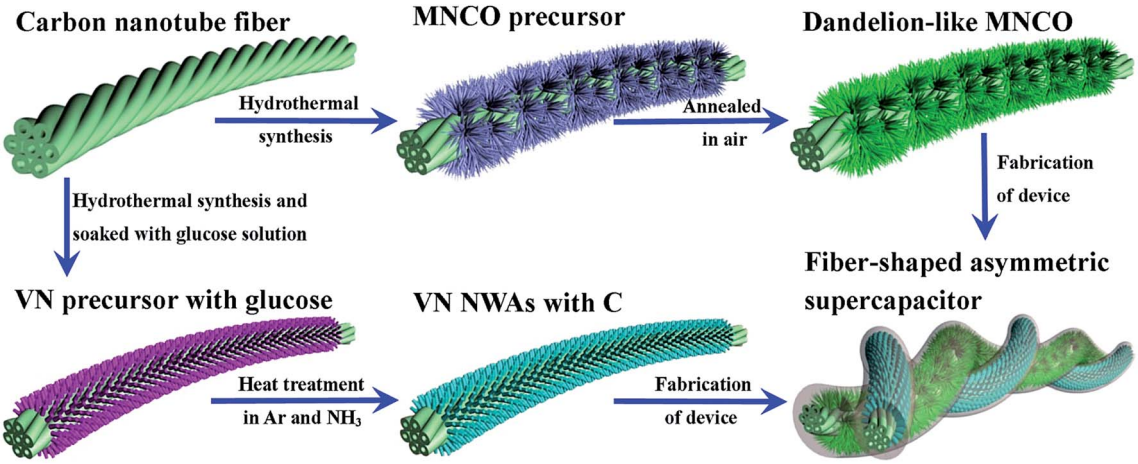

Fig. 3 Detailed schematic illustration of the fabrication process for our FASC device.

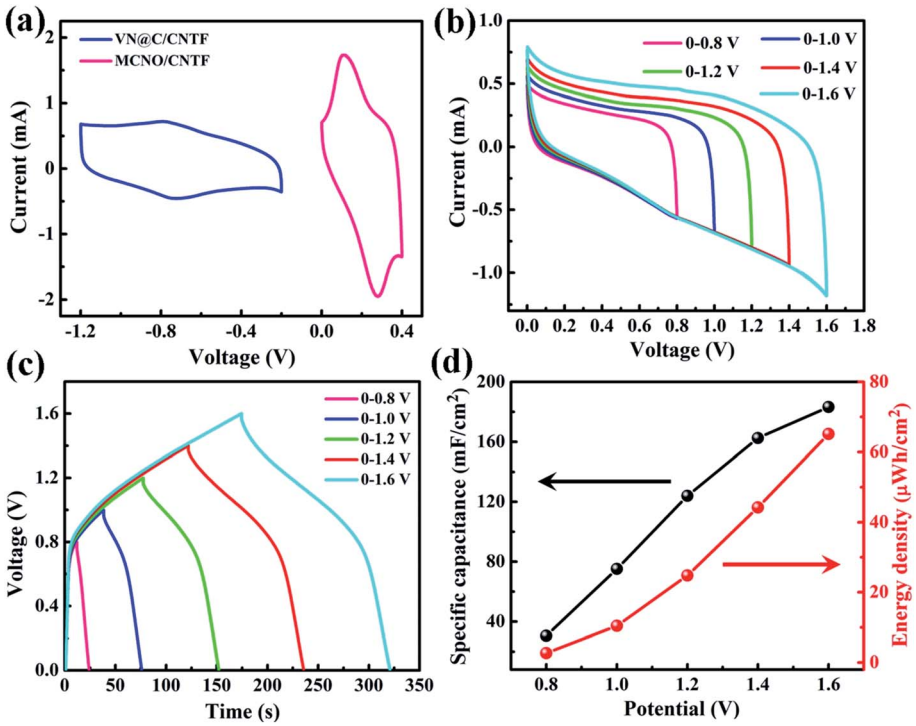

Fig. 4 Electrochemical characterization of our FASC device. (a) Comparative CV curves of the VN@C/CNTF and MNCO/CNTF electrodes at a scan rate of 5 mV s^{-1} in a three-electrode system in 3 M KOH aqueous solution. (b) CV curves of the device with different operating voltages at a constant scan rate of 25 mV s^{-1}. (c) GCD curves of the device collected at different voltages from 0.8 to 1.6 V at a current density of 2 mA cm^{-2}. (d) Areal specific capacitance and energy density calculated based on the GCD curves obtained at 2 mA cm^{-2}.

to 1.6 V. Fig. 4b displays the CV curves of the VN@C/CNTF//MNCO/CNTF FASC device in different potential windows at a constant scan rate of 25 mV s^{-1}. As expected, our device clearly exhibits rectangular CV curves even at a high potential window of up to 1.6 V. Moreover, the nearly symmetric GCD curves collected at 2 mA cm^{-2} even at an operating potential as high as 1.6 V suggest ideal capacitance characteristics and low equivalent series resistance of our device (Fig. 4c). Fig. 4d demonstrates the areal specific capacitances and energy densities of the FASC based on the GCD curves as a function of the potential window. With the voltage windows of the device extending from 0.8 to 1.6 V, the areal specific capacitance greatly increases from 30.5 to 183.2 mF cm^{-2} and the energy density significantly improves from 2.7 to 65.2 μW h cm^{-2}.

Fig. 5a presents the CV curves of the FASC device with the working voltage between 0 and 1.6 V at scan rates ranging from 5 to 80 mV s^{-1}. Note that all the curves maintain rectangular shapes even at a scan rate of 80 mV s^{-1}, demonstrating the exceptional capacitive behavior and fast charge–discharge properties of the FASC device. To further evaluate its electrochemical performance,

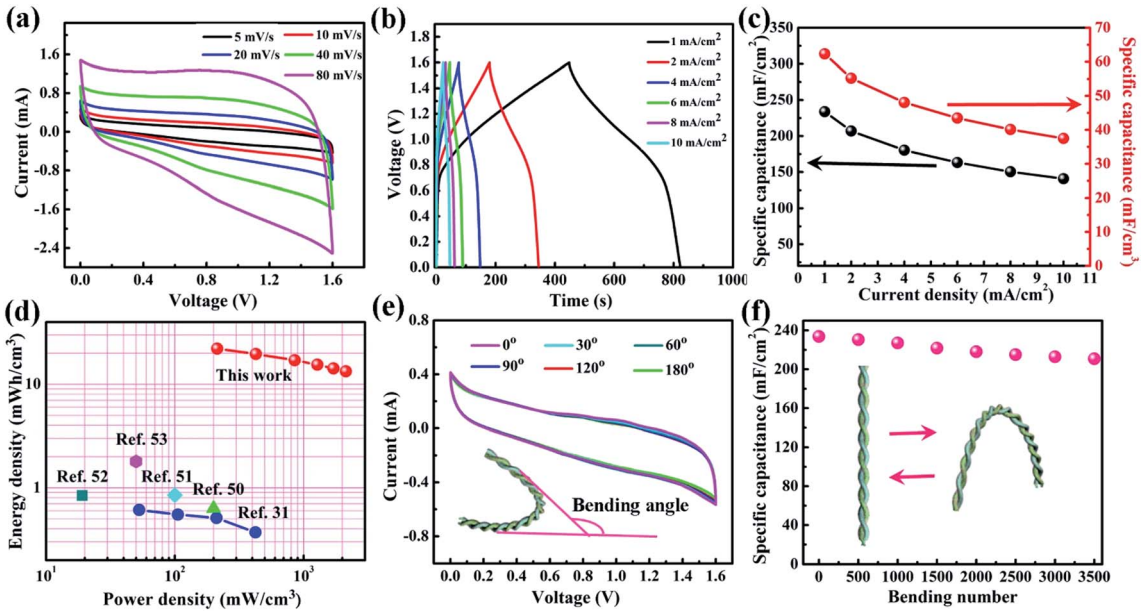

Fig. 5 (a) CV curves of the VN@C/CNTF//MNCO/CNTF FASC at scan rates ranging from 5 to 80 mV s^{-1} in the potential window of 0–1.6 V. (b) GCD curves collected at different current densities with the operating window of 1.6 V. (c) Areal and volumetric specific capacitance of the device calculated from the GCD curves as a function of current density. (d) Volumetric energy and power densities of our device in comparison with previously reported FASCs. (e) CV curves of the device measured at a scan rate of 5 mV s^{-1} under different bending angles. (f) Normalized capacitances of the as-obtained FASC with the bending angles of 90° for 3500 cycles.

GCD curves were collected at different current densities ranging from 1 to 10 mA cm^{-2}, as illustrated in Fig. 5b. The nearly symmetric curves again indicate the ideal pseudocapacitive properties and excellent reversibility of our device. Fig. 5c displays the areal and volumetric specific capacitance calculated from the corresponding GCD curves at different current densities. Significantly, the FASC device delivers a desirable specific capacitance of 62.3 F cm^{-3} (233.7 mF cm^{-2}) at a current density of 1 mA cm^{-2} and still retains a specific capacitance of 37.5 F cm^{-3} (140.6 mF cm^{-2}) even at a high current density of 10 mA cm^{-2}, indicating remarkable rate capability. Fig. 5d compares the volumetric energy and power densities of our devices to the values of previously reported FASCs. Owing to the extended operating voltage of 1.6 V and the high specific capacitance, our FASC device displays a remarkable energy density of 22.2 mW h cm^{-3} at a power density of 213.3 mW cm^{-3} and still retains an excellent energy density of 13.3 mW h cm^{-3} even at the high power density of 2133.3 mW cm^{-3}, considerably higher than those of previously reported FASCs, including Fe_2N@graphene nanosheets/carbon fiber//TiN@graphene nanosheets/carbon fiber (0.61 mW h cm^{-3} at 52.9 mW cm^{-3}),[31] graphene hydrogel/Cu wire//reduced graphene oxide@MnO_2/carbon fiber/(0.63 mW h cm^{-3} at 200 mW cm^{-3}),[50] CNT–$NiCo(OH)_x$/carbon fiber bundle//activated carbon/carbon fiber bundle (0.84 mW h cm^{-3} at 19.1 mW cm^{-3}),[51] CuO@AuPd@MnO_2/Cu wire//Fe_2O_3@carbon/carbon fiber (0.85 mW h cm^{-3} at 100 mW cm^{-3}),[52] self-standing WO_3@polypyrrole → graphene@polypyrrole/polished stainless wire (1.8 mW h cm^{-3} at 50 mW cm^{-3}).[53] Simultaneously, the areal energy and power densities of our device are illustrated in Fig. S12.† Fig. S13† shows the Nyquist plot of our device between the frequency of 10^{-2} and 10^5 Hz. The low equivalent series resistance (about 31.7 Ω) manifests low internal resistance and the nearly straight line in the low frequency region depicts the ideal capacitive behavior. The long-term cycling performance was measured by GCD analysis at a current density of 2 mA cm^{-2} (Fig. S14†). Our device demonstrates 89.7% capacitance retention after 3000 cycles, exhibiting outstanding cycling stability. It is very important to evaluate the flexibility and mechanical stability of the as-assembled FASC device for its potential application. As shown in Fig. 5e, the CV curves with negligible change under a variety of bending angles imply stable mechanical properties. Moreover, the capacitance of our device still retains 90.2% after 3500 bending cycles at a current density of 1 mA cm^{-2} (Fig. 5f), further confirming its intriguing flexibility.

Conclusion

In summary, hierarchical dandelion-like MNCO NWAs grown on CNTF with exceptional electrochemical performance have been successfully developed and directly used as an advanced positive electrode for high-performance asymmetric supercapacitors. Significantly, the MCNO/CNTF electrode demonstrates an ultrahigh specific capacitance of 490.7 F cm^{-3} (1840 mF cm^{-2}) at a current density of 1 mA cm^{-2}, ascribed to its unique three-dimensional nano-architecture and extraordinary conductivity. Furthermore, a high-performance and wearable FASC with a maximum operating window of 1.6 V has been successfully assembled by twisting the MNCO/CNTF positive electrode and VN@C/CNTF negative electrode together after coating them with a thin layer of KOH/PVA gel electrolyte.

Our FASC device exhibits a remarkable specific capacitance of 62.3 F cm^{-3} (233.7 mF cm^{-2}) and an exceeding energy density of 22.2 mW h cm^{-3} (83.1 μW h cm^{-2}). In addition, it possesses outstanding flexibility with the capacitance retention maintained at 90.2% after bending 3500 times. Thus, our work developed a feasible strategy to construct novel fiber electrodes for high-performance wearable fiber-shaped supercapacitors.

Conflicts of interest

There are no conflicts to declare.

Acknowledgements

This work was supported by the National Key R&D Program of China (No. 2017YFB0406000), the Key Research Program of Frontier Science of the Chinese Academy of Sciences (No. QYZDB-SSW-SLH031), the Natural Science Foundation of Jiangsu Province, China (No. BK20160399 and BK20140392), the Transformation of Scientific and Technological Achievements in Jiangsu Province (No. BA2016026), the Postdoctoral Foundation of Jiangsu Province (No. 1601065B), and the Science and Technology Project of Suzhou, China (No. SZS201508, ZXG201428 and ZXG201401).

Notes and references

1 M. F. El-Kady, S. Veronica, D. Sergey and R. B. Kaner, *Science*, 2012, **335**, 1326.
2 P. Yang, Y. Ding, Z. Lin, Z. Chen, Y. Li, P. Qiang, M. Ebrahimi, W. Mai, C. P. Wong and Z. L. Wang, *Nano Lett.*, 2014, **14**, 731.
3 S. Pan, H. Lin, J. Deng, P. Chen, X. Chen, Z. Yang and H. Peng, *Adv. Energy Mater.*, 2015, **5**, 1401438.
4 X. Lu, Y. Zeng, M. Yu, T. Zhai, C. Liang, S. Xie, M. S. Balogun and Y. Tong, *Adv. Mater.*, 2014, **26**, 3148–3155.
5 B. Anothumakkool, S. N. Bhange, R. Soni and S. Kurungot, *Energy Environ. Sci.*, 2015, **8**, 1339–1347.
6 L.-F. Chen, Z.-H. Huang, H.-W. Liang, W.-T. Yao, Z.-Y. Yu and S.-H. Yu, *Energy Environ. Sci.*, 2013, **6**, 3331–3338.
7 H. Chen, S. Zeng, M. Chen, Y. Zhang, L. Zheng and Q. Li, *Small*, 2016, **12**, 2035–2045.
8 Z. Pan, Y. Qiu, J. Yang, F. Ye, Y. Xu, X. Zhang, M. Liu and Y. Zhang, *Nano Energy*, 2016, **26**, 610–619.
9 J. Zhao, C. Li, Q. Zhang, J. Zhang, X. Wang, Z. Lin, J. Wang, W. Lu, C. Lu and C. P. Wong, *J. Mater. Chem. A*, 2017, **5**, 6928–6936.
10 M. Yu, D. Lin, H. Feng, Y. Zeng, Y. Tong and X. Lu, *Angew. Chem., Int. Ed.*, 2017, **129**, 5454–5459.
11 J. Ren, W. Bai, G. Guan, Y. Zhang and H. Peng, *Adv. Mater.*, 2013, **25**, 5965–5970.
12 X. Li, X. Li, J. Cheng, D. Yuan, W. Ni, Q. Guan, L. Gao and B. Wang, *Nano Energy*, 2016, **21**, 228–237.
13 Z. Li, M. Shao, L. Zhou, R. Zhang, C. Zhang, J. Han, M. Wei, D. G. Evans and X. Duan, *Nano Energy*, 2016, **20**, 294–304.
14 X. Dong, Z. Guo, Y. Song, M. Hou, J. Wang, Y. Wang and Y. Xia, *Adv. Funct. Mater.*, 2014, **24**, 3405–3412.
15 J. Yu, W. Lu, J. P. Smith, K. S. Booksh, L. Meng, Y. Huang, Q. Li, J. H. Byun, Y. Oh and Y. Yan, *Adv. Energy Mater.*, 2017, **7**, 1600976.
16 N. Yu, H. Yin, W. Zhang, Y. Liu, Z. Tang and M. Q. Zhu, *Adv. Energy Mater.*, 2016, **6**, 1501458.
17 D. Yu, K. Goh, Q. Zhang, L. Wei, H. Wang, W. Jiang and Y. Chen, *Adv. Mater.*, 2014, **26**, 6790–6797.
18 G. Sun, X. Zhang, R. Lin, J. Yang, H. Zhang and P. Chen, *Angew. Chem., Int. Ed.*, 2015, **54**, 4651–4656.
19 G. Qu, J. Cheng, X. Li, D. Yuan, P. Chen, X. Chen, B. Wang and H. Peng, *Adv. Mater.*, 2016, **28**, 3646–3652.
20 Q. Zhang, X. Wang, Z. Pan, J. Sun, J. Zhao, J. Zhang, C. Zhang, L. Tang, J. Luo and B. Song, *Nano Lett.*, 2017, **17**, 2719.
21 M. Li, M. Zu, J. Yu, H. Cheng and Q. Li, *Small*, 2017, **13**, 1602994.
22 X. Xia, J. Tu, Y. Mai, X. Wang, C. Gu and X. Zhao, *J. Mater. Chem.*, 2011, **21**, 9319–9325.
23 W. Ma, S. Chen, S. Yang, W. Chen, W. Weng, Y. Cheng and M. Zhu, *Carbon*, 2017, **113**, 151–158.
24 H. Chen, L. Hu, Y. Yan, R. Che, M. Chen and L. Wu, *Adv. Energy Mater.*, 2013, **3**, 1636–1646.
25 J. Yang, C. Yu, X. Fan, S. Liang, S. Li, H. Huang, Z. Ling, C. Hao and J. Qiu, *Energy Environ. Sci.*, 2016, **9**, 1299–1307.
26 Q. Ke, C. Guan, X. Zhang, M. Zheng, Y. W. Zhang, Y. Cai, H. Zhang and J. Wang, *Adv. Mater.*, 2017, **29**, 1604164.
27 S. Peng, L. Li, H. B. Wu, S. Madhavi and X. W. D. Lou, *Adv. Energy Mater.*, 2015, **5**, 1401172.
28 L. Sheng, T. Wei, Y. Liang, L. Jiang, L. Qu and Z. Fan, *Small*, 2017, **13**, 1700371.
29 X. Wang, B. Liu, R. Liu, Q. Wang, X. Hou, D. Chen, R. Wang and G. Shen, *Angew. Chem.*, 2014, **126**, 1880–1884.
30 M. Yu, X. Cheng, Y. Zeng, Z. Wang, Y. Tong, X. Lu and S. Yang, *Angew. Chem., Int. Ed.*, 2016, **55**, 6762–6766.
31 C. Zhu, P. Yang, D. Chao, X. Wang, X. Zhang, S. Chen, B. K. Tay, H. Huang, H. Zhang and W. Mai, *Adv. Mater.*, 2015, **27**, 4566–4571.
32 H. Jin, L. Zhou, C. L. Mak, H. Huang, W. M. Tang and H. L. W. Chan, *Nano Energy*, 2015, **11**, 662–670.
33 X. Xia, J. Tu, Y. Mai, X. Wang, C. Gu and X. Zhao, *J. Mater. Chem.*, 2011, **21**, 9319–9325.
34 D. Kong, J. Luo, Y. Wang, W. Ren, T. Yu, Y. Luo, Y. Yang and C. Cheng, *Adv. Funct. Mater.*, 2014, **24**, 3815–3826.
35 L. Shen, Q. Che, H. Li and X. Zhang, *Adv. Funct. Mater.*, 2014, **24**, 2736.
36 M. Kuang, Y. X. Zhang, T. T. Li, K. F. Li, S. M. Zhang, G. Li and W. Zhang, *J. Power Sources*, 2015, **283**, 270–278.
37 K. Qiu, M. Lu, Y. Luo and X. Du, *J. Mater. Chem. A*, 2017, **5**, 5820–5828.
38 T. Wang, Q. Le, G. Zhang, S. Zhu, B. Guan, J. Zhang, S. Xing and Y. Zhang, *Electrochim. Acta*, 2016, **211**, 627–635.
39 F. X. Ma, L. Yu, C. Y. Xu and X. W. D. Lou, *Energy Environ. Sci.*, 2016, **9**, 862–866.
40 G. Gao, H. B. Wu, S. Ding, L. M. Liu and X. W. D. Lou, *Small*, 2015, **11**, 804–808.
41 L. Shen, Q. Che, H. Li and X. Zhang, *Adv. Funct. Mater.*, 2014, **24**, 2630–2637.

42 D. Kong, W. Ren, C. Cheng, Y. Wang, Z. Huang and H. Y. Yang, *ACS Appl. Mater. Interfaces*, 2015, **7**, 21334–21346.
43 C. Wu, J. Cai, Q. Zhang, X. Zhou, Y. Zhu, P. K. Shen and K. Zhang, *ACS Appl. Mater. Interfaces*, 2015, **7**, 26512–26521.
44 S. Chen, G. Yang, Y. Jia and H. Zheng, *J. Mater. Chem. A*, 2017, **5**, 1028–1034.
45 L. Li, Y. Zhang, F. Shi, Y. Zhang, J. Zhang, C. Gu, X. Wang and J. Tu, *ACS Appl. Mater. Interfaces*, 2014, **6**, 18040–18047.
46 A. Maitra, A. K. Das, R. Bera, S. K. Karan, S. Paria, S. K. Si and B. B. Khatua, *ACS Appl. Mater. Interfaces*, 2017, **9**, 5947–5958.
47 M. Yu, S. Zhao, H. Feng, L. Hu, X. Zhang, Y. Zeng, Y. Tong and X. Lu, *ACS Energy Lett.*, 2017, **2**, 1862–1868.
48 D. Zheng, H. Feng, X. Zhang, X. He, M. Yu, X. Lu and Y. Tong, *Chem. Commun.*, 2017, **53**, 3929.
49 X. Lu, M. Yu, T. Zhai, G. Wang, S. Xie, T. Liu, C. Liang, Y. Tong and Y. Li, *Nano Lett.*, 2013, **13**, 2628–2633.
50 Z. Zhang, F. Xiao and S. Wang, *J. Mater. Chem. A*, 2015, **3**, 11215–11223.
51 X. Lu, Y. Bai, R. Wang and J. Sun, *J. Mater. Chem. A*, 2016, **4**, 18164–18173.
52 Z. Yu, J. Moore, J. Calderon, L. Zhai and J. Thomas, *Small*, 2015, **11**, 5289–5295.
53 Y. Huang, M. Zhu, Y. Huang, H. Li, Z. Pei, Q. Xue, Z. Liao, Z. Wang and C. Zhi, *J. Mater. Chem. A*, 2016, **4**, 4580–4586.